Ionics (2021) 27:2629–2638
https://doi.org/10.1007/s11581-021-04001-4

ORIGINAL PAPER

$La_{0.7}Sr_{0.3}CoO_3/Co_3O_4$ nanofibers with hollow network porous structure by one-step electrospinning for hybrid supercapacitor

Ling He[1,2] · Wenjuan Zheng[1,2] · Yao Shu[1,2] · Wensheng Li[1,2] · Maocheng Liu[2]

Received: 30 June 2020 / Revised: 16 February 2021 / Accepted: 8 March 2021 / Published online: 23 March 2021
© The Author(s), under exclusive licence to Springer-Verlag GmbH Germany, part of Springer Nature 2021

Abstract

Nanofibers with hollow or porous network structure have numerous prospective realistic applications in electrode materials of a hybrid supercapacitor. Herein, $La_{0.7}Sr_{0.3}CoO_3/Co_3O_4$ nanofibers (LSC/Co_3O_4 NFs) with hollow network porous structure where Co_3O_4 nanoparticles evenly distributed in the LSC single tube both sides of hollow are successfully prepared by one-step electrospinning. Electrochemical characteristics of LSC-doped composite electrode materials with different proportions have studied in detail. The result showed the LSC (20 wt%)/Co_3O_4 electrode material displayed the eminent specific capacity of 215 C g^{-1} (430 F g^{-1}) at 1 A g^{-1}. Furthermore, the LSC (20 wt%)/Co_3O_4//AC hybrid supercapacitor showed remarkable cyclic stability after 5000 cycles with a capacity retention of 86.3% and it showed a tremendous energy density of 21.9 Wh kg^{-1} at a power density of 358.4 W kg^{-1}. Hence, the prepared LSC/Co_3O_4 NFs have promised a new type of electrode for hybrid supercapacitors.

Keywords $La_{0.7}Sr_{0.3}CoO_3/Co_3O_4$ nanofibers · One-step electrospinning · Hollow network porous structure · Hybrid supercapacitor

Introduction

Hybrid supercapacitor is a novel kind of ecologically-gracious energy storage device with long life and high cycle efficiency while electrode materials are the key factors that affect the performance of capacitors [1–3]. As a significant member of transition metal oxide materials, Co_3O_4 has been extensively studied on account of its abundant redox activity and exhibits pseudo-capacitance behavior (theoretical capacitance is 3560 F g^{-1}) [4]. However, similar to other transition metal oxides, low electrode material utilization and poor conductivity are hindering their practical application [5–8]. Studies showed combining Co_3O_4 with high specific surface area material to form composite electrode material can extremely effectively improve the conductivity of Co_3O_4 and enhance the electrochemical properties, such as 3D graphene/Co_3O_4 electrode [9], Co_3O_4/PANI electrode [10], and Co_3O_4@PPy electrode [11]. However, the majority of the composites approach have been intricate the electrochemical performances, for example, specific capacitance and cyclic stability still necessitate to be improved [12, 13]. Recently, the perovskite-type oxide of the ABO_3 structure has been sizzling and researching on account of structural stability and electron-ion double conductivity [14, 15] and it is always coupled with other electrode materials [16–19] to applied in supercapacitor field [20, 21]. As one of the perovskite-type oxide materials, the $La_{0.7}Sr_{0.3}CoO_{3-\delta}$ has a remarkable electronic conductivity, although it can still reach 10^2~10^3 S cm^{-1} at room temperature according to report [17].

In recent years, increasing the specific surface area of electrode materials and reducing the ion transfer distance have been considered a new method to improve the electrochemical performance, of which the design of porous or hollow structures is a more commonly used method [5, 22, 23]. Electrospinning is a significantly successful strategy for the production of fibers with diameters from submicron to nanometer sizes, which also can prepare various graded nanostructures such as core-shell, hollow, and porous [24–26]. Electrospinning hollow porous nanofibers have received

✉ Ling He
hlswm@163.com

[1] State Key Laboratory of Advanced Processing and Recycling of Nonferrous Metals, Lanzhou University of Technology, Lanzhou 730050, Gansu, China

[2] School of Materials Science and Engineering, Lanzhou University of Technology, Lanzhou 730050, Gansu, China

considerable attention as potential electrode materials for hybrid supercapacitors because of their high conductivity, large specific surface area, and self-reliance.

In present work, LSC/Co_3O_4 NFs have been synthesized by doping with different proportions of LSC via one-step electrospinning technique. The electrochemical properties of LSC doped nano fibers with different concentrations have been studied for hybrid supercapacitor electrode material. The sample doped with 20 wt% exhibits most excellent electrochemical properties. The network connection mode of Co_3O_4 nanoparticles and LSC single tube not only promotes the electronic and ionic transport abilities but also ensures effective contact between the active substance and the electrolytes, bringing about an improved electrochemical performance.

Experimental section

Preparation of hollow network porous LSC/Co_3O_4 NFs

According to LSC/Co_3O_4 doped with different contents of LSC (LSC=0 wt%, 10 wt%, 20 wt%, 30 wt%, 50 wt%, 100 wt%), weighing different weights of $La(NO_3)_3$•$6H_2O$, $Sr(NO_3)_2$, and $Co(Ac)_2$•$4H_2O$ were all dissolved in 18 mL of *N*,*N*-dimethylformamide solvent. Then, 3.282 g of Polyvinyl pyrrolidone (K88-96) was added with stirring. The solution was stirred for 10 h to acquire a homogeneous purple sol at room temperature. The above-mixed sol was placed in a 20 mL plastic syringe, mounted on a syringe pump, and connected to a high voltage power source. The voltage, propulsion rate, and receiving distance for electrospinning are 15 kV, 0.3 mL/h, and 16 cm, respectively. The precursor fibers were collected and curing at 80 °C for 12 h and calcined at 600 °C for 5 h to obtain LSC/Co_3O_4 NFs. Figure 1 shows the process of preparing LSC/Co_3O_4 NFs by one-step electrospinning.

Material characterization

Determine the crystal phases of prepared samples by X-ray diffraction (XRD, D8 Advance). Scanning electron microscopy (SEM, JSM-6700F) with energy-dispersive X-ray spectrometry (EDS) and transmission electron microscopy (TEM, JEM-2010) is examined the morphology and characterization of the products. Additionally, the surface area of prepared samples and its pore size is checked by Nitrogen Adsorption Desorber (ASAP 2020). The state of chemical elements for samples is examined by XPS measurement (XPS, ES-CALAB 250 Xi).

Preparation of single electrode and hybrid device

To make a single working electrode, here use traditional slurry coating method. First, the active material (LSC/Co_3O_4 NFs), conductive agent acetylene black, and graphite are mixed uniformly in the ratio of 80 wt%, 7.5 wt%, and 7.5 wt%, and then, 5 wt% of PTFE emulsion and a few drops of alcohol are added to prepare a uniform slurry material. Secondly, it is coated on the foamed nickel that has been pretreated, the coating area is 1 cm^2, and the mass of the active material is 4 mg. Coat on nickel foam and dry at 60 °C for 12 h, eventually subjected to a series of electrochemical tests after being pressurized at 10 MPa for 3 min. The hybrid capacitor device is assembled by AC and LSC/Co_3O_4 coated on foam nickel as the negative electrode and the positive electrode, respectively. The preparation method of AC electrode is to mix activated carbon, PTFE, and conductive agent [27, 28] in a ratio of 80 wt%, 5 wt%, and 15 wt% evenly to form a viscous paste [17, 29–31]. Then, the paste was evenly coated on the foam nickel and placed in a drying oven at 60 °C for 12 h. Finally, the electrode is made by pressing the electrode under the pressure of 10 Mpa. The loading masses of LSC/Co_3O_4 and AC on nickel foam are 4 mg and 8 mg [32], respectively, calculated by the following equation [33]:

$$\frac{m_+}{m_-} = \frac{C_-\Delta V_-}{C_+\Delta V_+} \quad (1)$$

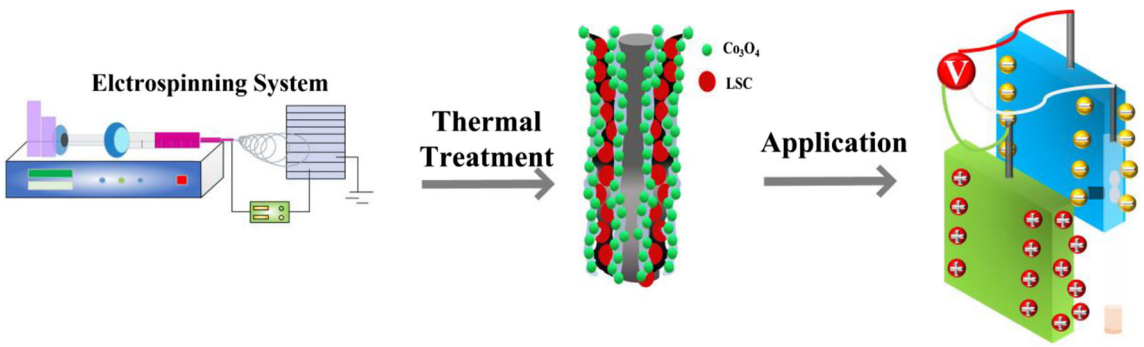

Fig. 1 Schematic illustration of the formation process of LSC/Co_3O_4 NFs with hollow network porous structure

where m (g) is the mass of the electrode material, and C (F g^{-1}) is specific capacity and $\triangle V$ (V) is cell voltage.

Electrochemical measurements

The electrochemical properties are tested at room temperature in a CHI660D electrochemical work station using6 M KOH as an electrolyte. In the three-electrode system, with LSC/Co_3O_4 NFs as the working electrode, Pt as the opposite electrode, Hg/HgO as the reference electrode. The cyclic voltammetry (CV), galvanostaic charging/discharge (GCD), and electrochemical impedance spectroscopy (EIS) were successively performed. In the meantime, a cycle stability test is carried out in the LAND system. The specific capacity (Q, C g^{-1}) can be calculated from GCD curve according to the follow equation [34]:

$$Q = \frac{I \times t}{m} \tag{2}$$

Here I (A) corresponds to the charging and discharging current of the electrode material, t (s) represents the discharge time, and m (g) is the mass of the active material.

When assembling the hybrid device, the specific capacitance (C, F g^{-1}) can be calculated from the GCD curve, and the energy density (E, Wh kg^{-1}) and power density (P, W kg^{-1}) can be calculated using the following equations [35]:

$$C = \frac{I \times \Delta t}{m \times \Delta V} \tag{3}$$

$$E = \frac{1}{2} C (\Delta V)^2 \tag{4}$$

$$P = \frac{E}{\Delta t} \tag{5}$$

Here I (A) corresponds to the charging and discharging current of the electrode material, Δt (s) represents the discharge time, m (g) is the mass of the active material, and ΔV (V) stands for cell voltage.

Results and discussion

Morphology and structure characterization

SEM and TEM were used to characterize the morphology and structure of LSC/Co_3O_4 NFs. As shown in Fig. 2a, the PVP/$La_{0.7}Sr_{0.3}$Co-O precursor fibers show a continuous state with a very smooth surface and no fracture, its diameter about 350 nm. The diameter of the calcined LSC/Co_3O_4 NFs was reduced to about 140–190 nm put down to the evaporation of PVP, H_2O, and organics [19, 25], as presented in Fig. 2b–e. Simultaneously, Fig. 2b–e depicts the SEM images of LSC/Co_3O_4 with LSC content of 10 wt%, 20 wt%, 30 wt%, and 50 wt%, respectively. It can be seen from the figure that all fibers have a rough surface due to the formation of pores. When the LSC ratio is 10 wt%, the pores on the fiber surface are not uniformly distributed. The LSC (20 wt%)/Co_3O_4 has a hemp flowers shape with abundant pores and uniform fiber arrangement. However, when the content of LSC increases, agglomeration will occur between the fibers, and it is even difficult to maintain the fiber shape. Figure 2f shows the overall morphology of the fibers, indicating that LSC/Co_3O_4 composite nanofibers prepared by one-step electrospinning method have one-dimensional fiber morphology. Figure 2g shows the SEM images of section structure LSC/Co_3O_4 NFs and it can be clearly seen that one-dimensional nanofibers have hollow structures. The average wall thickness of the hollow nanofiber is 50 nm, and the hollow diameter is about 90 nm. The formation of hollow structure can be attributed to the roasting process, which has great influence on the final crystallization and structure development of hollow nanofibers [36–38]. The LSC/Co_3O_4 gelatinous shell is first obtained by electrospinning, and the fibers exposed to the air form an oxide layer during heat treatment, but for the inner fiber, a lack of oxygen prevents the salt from breaking down into its corresponding oxide. With the increase of heat treatment temperature, different concentration gradients drive the remaining salt to migrate from the inner fiber to the surface, forming LSC/Co_3O_4 inorganic particle powder and finally forming hollow inorganic nanofibers.

A typical hollow structure in the TEM imagines of composite fibers can be exhibited in Fig. 2h. It was worth noting that Co_3O_4 (green square) evenly attached to both sides of the LSC (red square) single tube with uniform thickness, forming a network porous structure. In addition, Fig. 2i presents the HRTEM image of the green and red regions in Fig. 2h, which the lattice fringes were significant visible, and the inter-planar spacing was 0.165 nm and 0.268 nm, which can be corresponded to the (422) plane of Co_3O_4 and (104) plane of LSC, respectively. The PVP/$La_{0.7}Sr_{0.3}$Co-O precursor synthesized by the sol-gel method is uncrystaline state and requires further annealing to realize the perovskite structure. When heat treatment is in the air, the precursor begins to crystallize at about 200 °C. When the annealing temperature rises to 600 °C, Co ions segregate at the LSC-O crystal interface and form a Co_3O_4 heterostructure [39–41]. Moreover, the EDS results (Fig. S1b) from the fiber surface (Fig. S1a) confirmed the La and Sr elements were mainly located on core and the O element was uniformly situated across the entire structure, while the Co element focused on the surface of the single tube. These results showed that Co_3O_4 nanoparticles were evenly distributed on the LSC framework, forming a high porosity, which not only made electrons transfer faster, but also shortened the electron transfer path.

Figure 3 is an XRD pattern of LSC/Co_3O_4 composites doped with different amounts of LSC. It could be seen from the picture that the Co_3O_4 diffraction peak exhibited by the

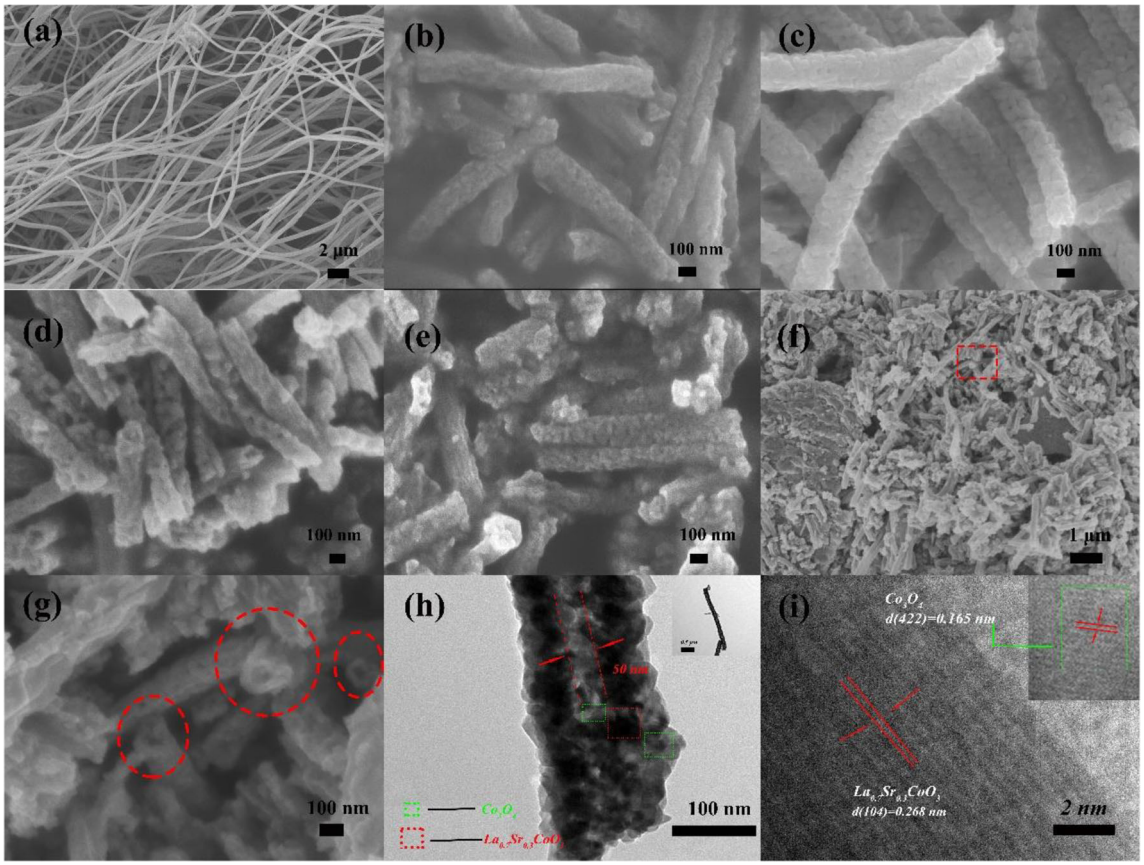

Fig. 2 **a** SEM images of the PVP/$La_{0.7}Sr_{0.3}Co$-O precursor. **b**–**e** SEM images of LSC (10 wt%)/Co_3O_4 NFs, LSC (20 wt%)/Co_3O_4 NFs, LSC (30 wt%)/Co_3O_4 NFs, and LSC (50 wt%)/Co_3O_4 NFs, respectively. **f** SEM of LSC/Co_3O_4 overall morphology. **g** SEM images of section structure of LSC/Co_3O_4 NFs. **h** TEM images of product with hollow network porous structure and **i** HRTEM image

20 wt% doping amount is higher than that of other doping amounts, which is consistent with the optimal content result

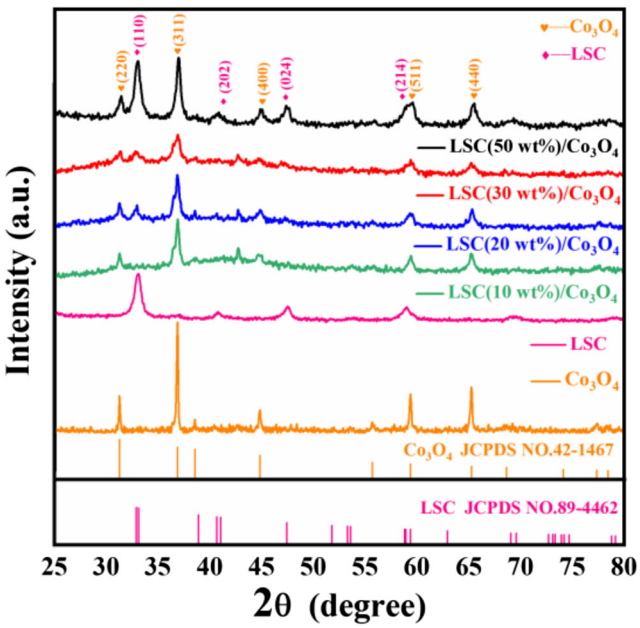

Fig. 3 XRD patterns of LSC/Co_3O_4 NFs with different LSC content

obtained from the electrochemical performance test. For different proportions of LSC/Co_3O_4, there were six distinctive peaks at 19.00°, 31.27°, 36.85°, 44.80°, 59.35°, and 65.23° in the XRD pattern, aparting from the diffraction peaks of LSC, which corresponded to the crystal planes of (111), (220), (311), (400), (511), and (440) of the Co_3O_4 phase (JCPDS No.42-1467), respectively. No other peaks are observed, which means that the LSC/Co_3O_4 composite has been successfully prepared by electrospinning.

Figure 4a exhibits the N_2 sorption-desorption and resultant pore size distributions curves of LSC (20 wt%)/Co_3O_4 NFs sample, which had the higher BET specific surface area of about 30.73 $m^2\ g^{-1}$ than LSC (26.02 $m^2\ g^{-1}$). The pore size distributions acquired by the BJH model verified the mesoporous feature with the main peak centered between 2.01 to 4.24 nm. In comparison, the optimal pore size distribution range is 2–5 nm, which is larger than the size of the electrolyte ions [42]. The curve was of type IV with the obvious hysteresis loops, telling the mesoporous structure [43]. These results showed that the prepared composites not only have increased surface area but also have abundant hollow and mesoporous, which is profit from the diffusion of electrolyte ions. The full-survey-scan XPS spectrum can explain the existence of La, Sr,

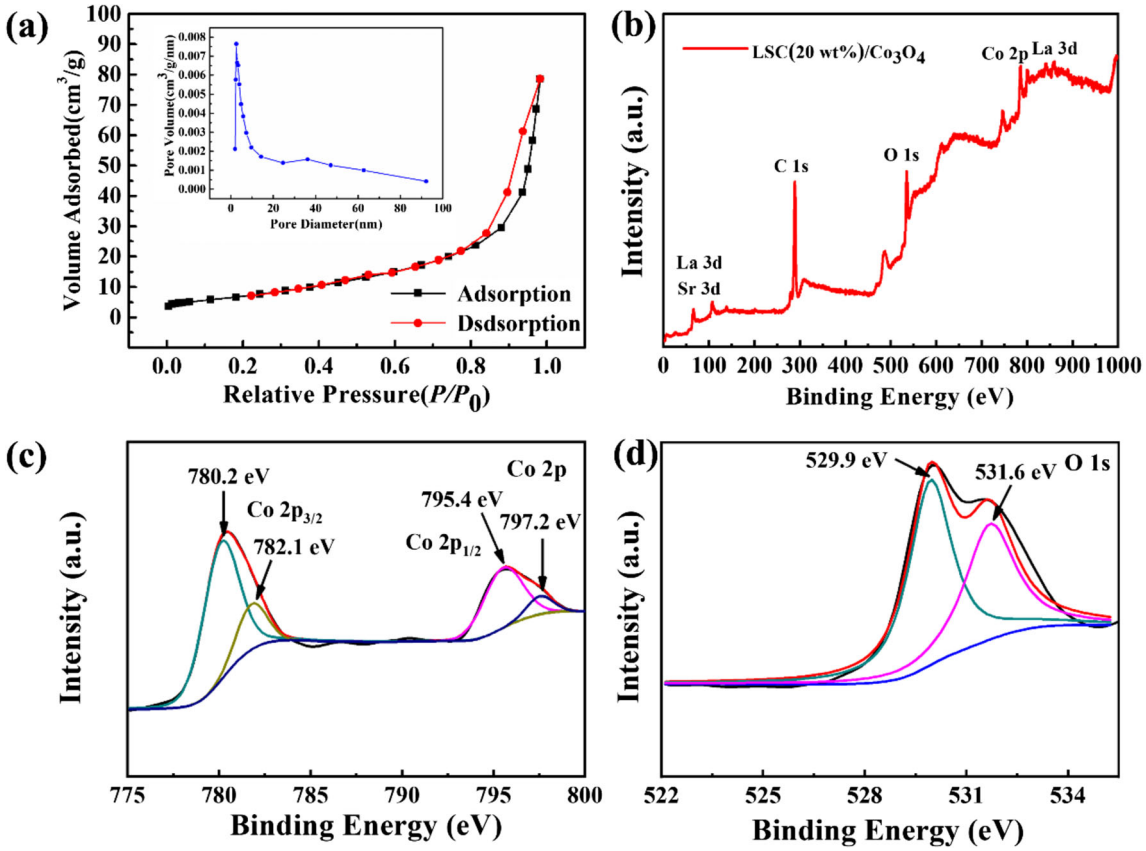

Fig. 4 **a** Nitrogen adsorption−desorption isotherm of the LSC (20 wt%)/Co_3O_4 NFs and the inset corresponding pore size distributions. **b** XPS spectrum of survey spectrum. **c** Co 2p and **d** O 1s

Co, and O, as can be observed from Fig. 4b. There are four peaks can be seen in the high-resolution Co 2p spectrum (Fig. 4c). The peaks at 797.2 eV (Co 2p $_{1/2}$) and 780.2 eV (Co 2p $_{3/2}$) were attributed to the chemical state of Co^{2+} while those at 795.4 eV (Co 2p $_{1/2}$) and 782.1 eV (Co 2p $_{3/2}$) were assigned to Co^{3+} [44, 45], respectively. Meanwhile, for the O 1s core-level spectra shown in Fig. 4d, there was one peak at 529.9 eV, corresponding to Co_3O_4 in the sample, and another peak at 531.6 eV was associated with surface hydroxyl groups of the sample [8, 46]. The XPS results further bear out the existence of Co_3O_4 and LSC phases in the prepared LSC (20 wt%)/Co_3O_4 NFs.

Electrochemical performances of prepared LSC/Co_3O_4

Figure 5a shows the comparative CV curves of pure Co_3O_4 electrode, pure LSC electrode, and LSC/Co_3O_4 electrodes with different LSC contents at a scan rate of 20 mV s^{-1}. Generally, the specific capacity of the electrode material is determined by the area of the CV. The results bring to light that the specific capacity of the LSC (20 wt%)/Co_3O_4 higher than that of other samples. Figure 5b illustrates that the discharge time of LSC (20 wt%)/Co_3O_4 is longer than other electrodes when the current density is 1 A g^{-1}. Furthermore, all discharge curves showed an approximate plateau rather than linear curves standing for the distinct capacitor, which further indicates the typical Faradic (battery-type electrode) redox reaction characteristic [47, 48]. Based on this result, we can conclude from the electrochemical performance shown by the trends of CV and GCD curves that the optimal doping amount of LSC is 20 wt%. This phenomenon is mainly attributed to the morphological structure of the composite nanofiber. It can be seen from the SEM images of LSC/Co_3O_4 doped with different contents that when the doped amount of LSC is less than 20 wt%, it is difficult to form holes on the surface due to the accumulation of Co_3O_4 particles. When the doping amount of LSC is 20 wt%, uniform pores are formed and the fibers are arranged neatly. The electrolyte easily penetrates into the porous electrode material, and the oxidation-reduction reaction occurs. At the same time, more Co_3O_4 provides a larger specific capacitance, so that LSC (20 wt%)/Co_3O_4 achieves the best specific capacitance.

The CV curve of the LSC (20 wt%)/Co_3O_4 single electrode displayed symmetric and gradually enhanced redox peaks at a scan rate of 5 to 100 mV s^{-1}, as shown in Fig. 5c, suggesting outstanding reversibility after the introduction of LSC thank the synergistic effect between LSC and Co_3O_4. With the expansion of scan rates, the redox flows continuously upgrade,

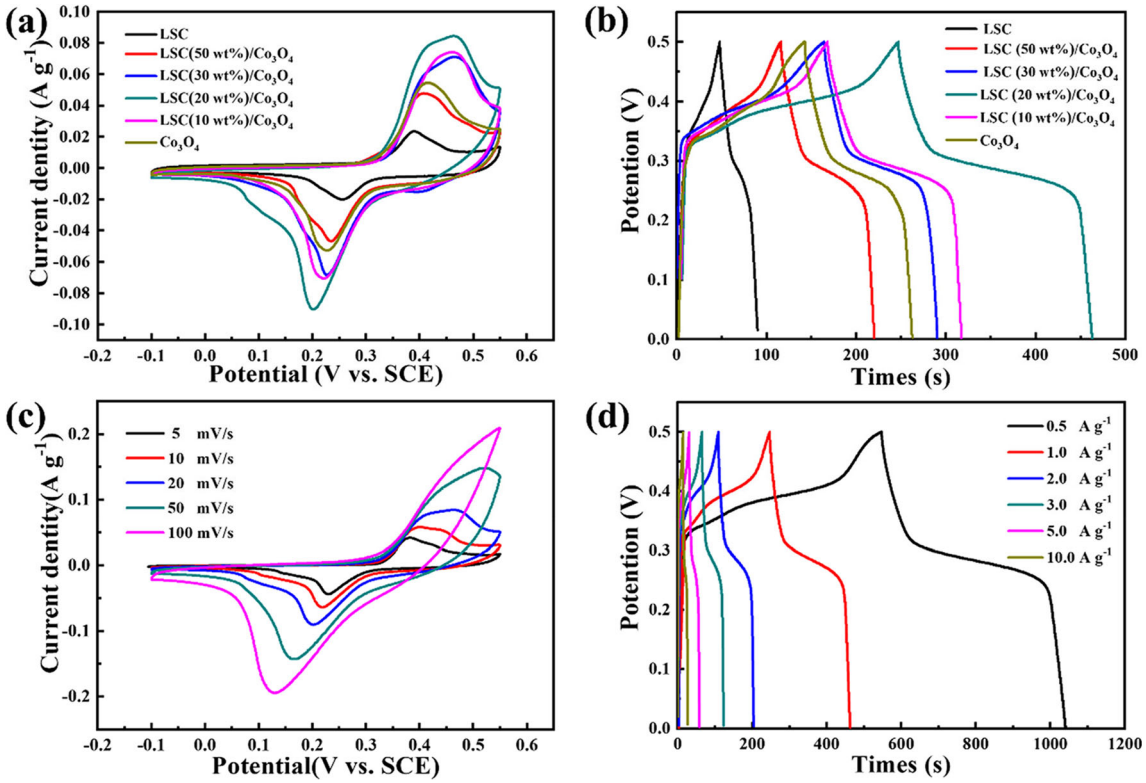

Fig. 5 **a**–**b** Electrochemical characterization of pure LSC, LSC/Co_3O_4 with different doping content LSC, pure Co_3O_4 electrodes **a** CV curves at 20 mV s^{-1}. **b** GCD curves at a current density of 1 A g^{-1}. **c**–**d** Electrochemical characterization of LSC (20 wt%)/Co_3O_4 electrode **a** CV curves. **d** GCD curves

and the oxidation tops were moved towards positive potential, in contrast the decrease tops moved towards negative potential, which uncovered good electrochemical reversibility of the oxidation-decrease forms. The redox responses of the LSC (20 wt%)/Co_3O_4 electrode material as follows [44, 49]. Figure 5d displays the GCD profiles at a high current density from 0.5 to 10 A g^{-1}. The consequence suggested that the LSC (20 wt%)/Co_3O_4 possessed good super capacitive behaviors, which corresponded with those results attained from CV analysis.

$$Co_3O_4 + OH^- + H_2O \leftrightarrow 3CoOOH + e^- \quad (6)$$

$$CoOOH + OH^- \leftrightarrow CoO_2 + H_2O + e^- \quad (7)$$

Figure 6a shows the specific capacitance of LSC/Co_3O_4 doped with different proportions of LSC, which could be clearly observed that the LSC (20 wt%)/Co_3O_4 revealed the largest specific capacitance with different current densities among those samples. The EIS was performed at 0.01-10^5 Hz to further analyze the electrochemical kinetics of the LSC (20 wt%)/Co_3O_4 composite electrodes, as shown in Fig. 6b. Compared with the pure Co_3O_4 electrode and the pure LSC electrode, the LSC (20 wt%)/Co_3O_4 electrode had lower transfer resistance and diffusion resistance, suggesting exist high capacitance. At the same time, we also carried out the electronic conductivity test of the sample, which was 241 s/cm.

The effect of different LSC content on the specific capacitance of LSC/Co_3O_4 electrode was shown in Fig. 6c. This image indicated that the specific capacitance of the LSC/Co_3O_4 electrode obviously improved with the increasing proportion of LSC when X (LSC content) < 20 wt%. Oppositely, when X > 20 wt%, the specific capacity of the LSC/Co_3O_4 electrode decreased with the increase of LSC content, and the maximum specific capacity of 215 C g^{-1} (430 F g^{-1}) achieved in LSC (20 wt%)/Co_3O_4, which was nearly twice that of the pure Co_3O_4 electrode and more than 5 times that of the LSC electrode. We supposed this result was caused by the addition of an appropriate amount of LSC and the hollow porous network structure to promote the transport of electrons. It can be seen in Fig. 6d that the LSC (20 wt%)/Co_3O_4 electrode was subjected to a constant current charge-discharge for 5000 cycles at a current density of 1 A g^{-1}, which exhibited capacitive retention of 95.3%. Remarkably, the LSC (20 wt%)/Co_3O_4 composite electrode material was superior to those similar materials reported in the literature, as shown in Table S2.

Additionally, electrochemical characteristics of the LSC (20 wt%)/Co_3O_4 composites for valid uses of a hybrid device

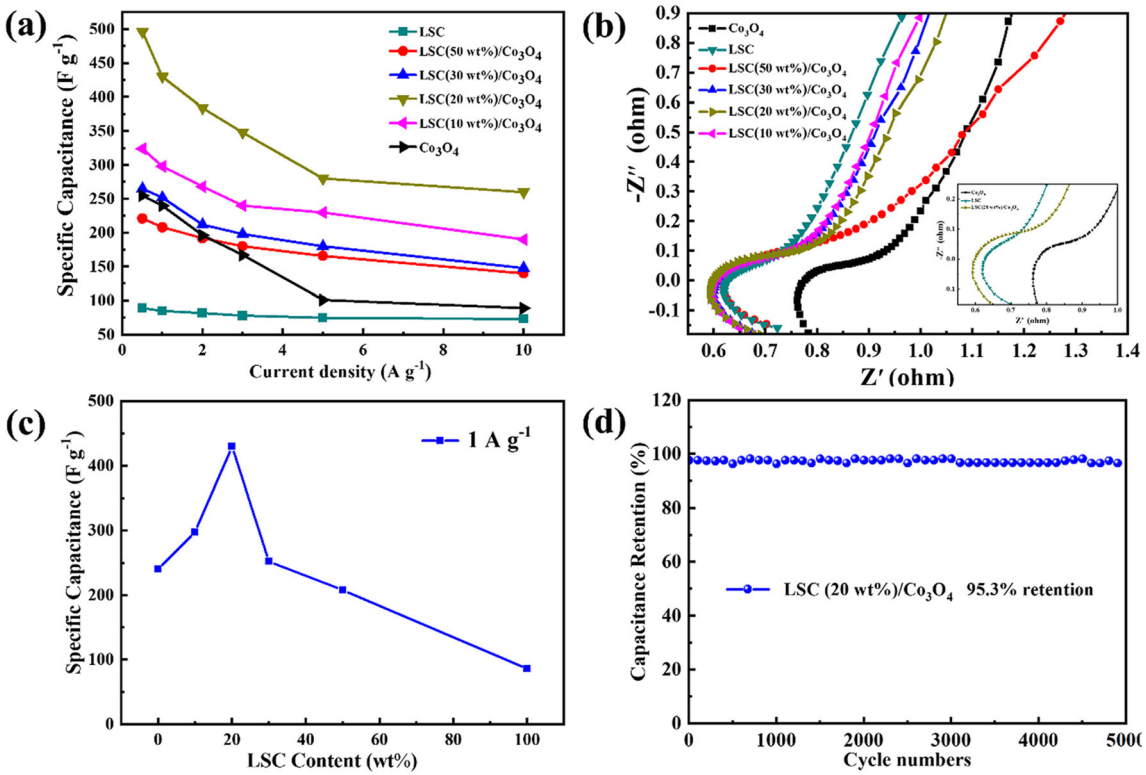

Fig. 6 **a** Rate capability of LSC/Co_3O_4 with different LSC content. **b** EIS curves of the LSC, Co_3O_4, and LSC (20 wt%)/Co_3O_4 electrodes materials. **c** Variation of specific capacity of different LSC content. **d** Cycling stability of LSC (20 wt%)/Co_3O_4 electrode at 1 A g^{-1}

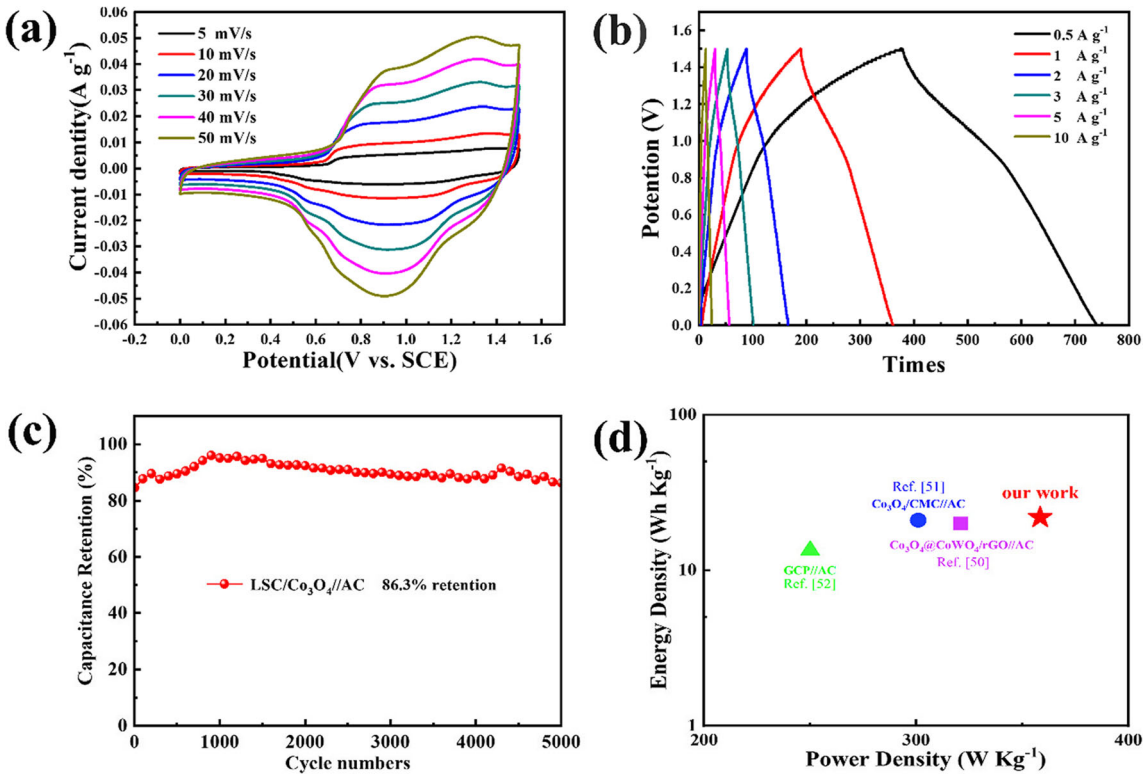

Fig. 7 Electrochemical performance of the LSC (20 wt%)/Co_3O_4//AC hybrid device: **a** CV curves. **b** GCD curves. **c** Cycling stability performance. **d** Ragone plots

were created with an AC mode as negative electrode and the LSC (20 wt%)/Co_3O_4 composites as a positive electrode. Figure 7a demonstrates the CV curves of hybrid device in potential window ranges of 0–1.5 V. Moreover, it can be found that the CV curve had a rectangular appearance of the electric double layer capacitor, attributing to the negative material AC belongs to double-layer capacitor material. In addition, when the scan rate reached 50 mV s^{-1}, the CV curve still showed a similar shape, which indicated the excellent reversibility of the hybrid device. Furthermore, the potential window of the LSC/Co_3O_4 single electrode is 0.5 V, while the potential window of the capacitor is 1.5 V when assembled into the hybrid device.

Figure 7b depicts the GCD curves of the hybrid device at various current densities, represents symmetrical triangular shapes revealing an ideal capacitive behavior. In order to get the specific capacitance of the hybrid device, the specific capacitances have been calculated from GCD curves and found to be 70, 64.7, 60.2, 54.7, 52.6, and 46 F g^{-1} at the current densities of 0.5, 1, 2, 3, 5, and 10 A g^{-1}, respectively. The cyclic stability of the LSC (20 wt%)/Co_3O_4//AC supercapacitor was appeared in Fig. 7c. The specific capacitance of the LSC (20 wt%)/Co_3O_4//AC hybrid device remained at 86.3% after 5000 cycles, demonstrating the consistency in cycling ability. The LSC (20 wt%)/Co_3O_4//AC hybrid device exhibits 21.9 Wh kg^{-1} and 358.4 W kg^{-1} energy and power densities respectively. Figure 7d shows a comparison of Ragone plots between our work and other works. The Ragone plots are to compare the performance of the energy storage device. As can be seen from Fig. 7d, the power density and energy density of our work are better than some reported work in recent years [50–52]. It additionally displayed a wonderful electrochemical reversibility and realistic energy densities, signifying that the LSC (20 wt%)/Co_3O_4 composites are prospective electrode materials for hybrid supercapacitor.

Conclusions

In summary, the novel hollow network porous LSC/Co_3O_4 NFs with different LSC contents were successfully synthesized via the one-step electrospinning method. It is found that doping LSC with appropriate content can significantly improve the electrochemical performance of composite electrode materials. The hollow network porous LSC (20 wt%)/Co_3O_4 NFs exhibited a high specific capacity of 215 C g^{-1} at current densities of 1 A g^{-1}, and showed outstanding cycling stability (capacitance retention retains 86.3% after 5000 cycles at 1 A g^{-1}). Furthermore, LSC (20 wt%)/Co_3O_4//AC hybrid device exhibits an energy density of 21.9 Wh kg^{-1} with a power density of 358.4 W kg^{-1}, indicating the potential of the LSC (20 wt%)/Co_3O_4 composites electrode in electrochemical energy storage applications. These results indicate that LSC/Co_3O_4 NFs is a potentially advantageous electrode material in the field of hybrid supercapacitors.

Supplementary Information The online version contains supplementary material available at https://doi.org/10.1007/s11581-021-04001-4.

Acknowledgements This work thanks to the Shenyang National Research Center for Materials Science and State Key Laboratory of Advanced Processing and Recycling of Non-Ferrous Metals [18LHPY006], the National Natural Science Foundation of China [51674130], and the Key Research and Development of Gansu Province, China [17JR7GA014].

Declarations

Competing interests The authors declare no competing interests.

References

1. Liu H, Liu X, Wang SL, Liu HK, Li L (2020) Transition metal based battery-type electrodes in hybrid supercapacitors: a review. Energy Stor Mater 28:122–145
2. Liu MC, Xu Y, Hu YX, Yang QQ, Kong LB, Liu WW, Niu WJ, Chueh YL (2018) Electrostatically charged MoS_2/graphene oxide hybrid composites for excellent electrochemical energy storage devices. ACS Appl Mater Interfaces 10:35571–35579
3. Afif A, Rahman SMH, Azad TA, Zaini J, Islan MA, Azad AK (2019) Advanced materials and technologies for hybrid supercapacitors for energy storage – a review. J Energy Stor 25: 100852
4. Guo XT, Zhang GX, Li Q, Xue HG, Pang H (2018) Non-noble metal-transition metal oxide materials for electrochemical energy storage. Energy Stor Mater 15:171–201
5. Wei JL, Li XR, Xue HG, Shao JY, Zhu RM, Pang H (2018) Hollow structural transition metal oxide for advanced supercapacitors. Adv Mater Interfaces 5:170159
6. Wang YL, Ma RX, Liu LZ, Xu ZC, Li FH (2017) A facile one-pot method for co_3o_4/graphene composite as efficient electrode materials for supercapacitors. Nano Brief Rep Rev 12:1750102
7. Wang JY, Dou W, Zhang XT, Han WH, Mu XM, Zhang Y, Zhao XH, Chen YX, Yang ZW, Su Q, Xie EQ, Lan W, Wang XR (2017) Embedded Ag quantum dots into interconnected Co_3O_4 nanosheets grown on 3D graphene networks for high stable and flexible supercapacitors. Electrochim Acta 224:260–268
8. Huang J, Xu YZ, Xiao YB, Zhu H, Wei JC, Chen YW (2017) Mussel-inspired, biomimetics-assisted self-assembly of Co_3O_4 on carbon fibers for flexible supercapacitors. ChemElectroChem 4: 2269–2277
9. Yang MH, Choi BG (2017) Preparation of three-dimensional Co_3O_4/graphene composite for high-performance supercapacitors. Chem Eng Commun 204:723–728
10. Ren XH, Fan HQ, Ma JW, Wang C, Zhang MC, Zhao N (2018) Hierarchical Co_3O_4/PANI hollow nanocages: synthesis and application for electrode materials of supercapacitors. Appl Surf Sci 441: 194–203
11. Yang XJ, Xu KB, Zou RJ, Hu JQ (2016) A hybrid electrode of Co_3O_4@PPy core/shell nanosheet arrays for high-performance supercapacitors. Nano-Micro Lett 8:143–150

12. Bao YX, Deng Y, Wang M, Xiao ZY, Wang MH, Fu YL, Guo ZY, Yang Y, Wang L (2020) A controllable top-down etching and in-situ oxidizing strategy: metal-organic frameworks derived α-Co/$Ni(OH)_2$@Co_3O_4 hollow nanocages for enhanced supercapacitor performance. Appl Surf Sci 504:144395
13. Liu XX, Wu R, Wang Y, Xiao SH, He Q, Niu XB, Blackwood DJ, Chen JS (2019) Self-supported core/shell Co_3O_4@Ni_3S_2 nanowires for high-performance supercapacitors. Electrochim Acta 311:221–229
14. Mefford JT, Hardin WG, Dai S, Keith PJ, Keith JS (2014) Anion charge storage through oxygen intercalation in $LaMnO_3$ perovskite pseudocapacitor electrodes. Nat Mater 13:726–732
15. Grenier JC, Pouchard M, Wattiaux A (1996) Electrochemical synthesis: oxygen intercalation. Curr Opin Solid State Mater Sci 1: 233–240
16. Galal A, Hassan HK, Atta NF, Jacob T (2019) Energy and cost-efficient nano-Ru-based perovskites/RGO composites for application in high performance supercapacitors. J Colloid Interface Sci 538:578–586
17. Liu PP, Liu J, Cheng S, Cai WZ, Yu FY, Zhang YP, Wu P, Liu ML (2017) A high-performance electrode for supercapacitors: silver nanoparticles grown on a porous perovskite-type material $La_{0.7}Sr_{0.3}CoO_{3-\delta}$ substrate. Chem Eng J 328:1–10
18. Liu X, Du G, Zhu JL, Zeng ZF, Zhu XH (2016) NiO/$LaNiO_3$ film electrode with binder-free for high performance supercapacitor. Appl Surf Sci 384:92–98
19. Hu L, Deng YF, Liang K, Liu XJ, Hu WC (2014) $LaNiO_3$/NiO hollow nanofibers with mesoporous wall: a significant improvement in NiO electrodes for supercapacitors. J Solid State Electrochem 19:629–637
20. Orlovskaya N, Gogotsi Y, Reece M, Chen BL, Gibson I (2002) Ferroelasticity and hysteresis in $LaCoO_3$ based perovskites. Acta Mater 50:715–723
21. Zhang SG, Han N, Tan XY (2015) Density functional theory calculations of atomic, electronic and thermodynamic properties of cubic $LaCoO_3$ and $La_{1-x}Sr_xCoO_3$ surfaces. RSC Adv 5:760–769
22. Chen LF, Lu Y, Yu L, Lou XW (2017) Designed formation of hollow particle-based nitrogen-doped carbon nanofibers for high-performance supercapacitors. Energy Environ Sci 10:1777–1783
23. Miao YE, Fan W, Chen D, Liu T (2013) High-performance supercapacitors based on hollow polyaniline nanofibers by electrospinning. ACS Appl Mater Interfaces 5:4423–4428
24. Sun GR, Sun LQ, Xie HM, Liu J (2016) Electrospinning of nanofibers for energy applications. Nanomaterials 6:129
25. Li Y, Wu H, Wu Y, Li Q (2017) Facile synthesis of mesoporous Co_3O_4 nanowires for application in supercapacitors. J Mater Sci: Mater Elecctron 28:16826–16835
26. Liu Q, Zhu J, Zhang L, Qiu Y (2018) Recent advances in energy materials by electrospinning. Renew Sust Energ Rev 81:1825–1858
27. Laheäär A, Przygocki P, Abbas Q, Béguin F (2015) Appropriate methods for evaluating the efficiency and capacitive behavior of different types of supercapacitors. Electrochem Commun 60:21–25
28. Naoi K, Ishimoto S, Miyamoto J, Naoi W (2012) Second generation 'nanohybrid supercapacitor': evolution of capacitive energy storage devices. Energy Environ Sci 5:9363–9373
29. Yan ZY, Guo CL, Yang F, Zhang CC, Mao YQ, Cui SX, Wei YH, Hou LF, Xu LH (2017) Cliff-like NiO/Ni_3S_2 directly grown on Ni foam for battery-type electrode with high area capacity and long cycle stability. Electrochim Acta 251:235–243
30. Chen LN, Zhai W, Chen L, Li DP, Ma XX, Ai Q, Xu XY, Hou GM, Zhang L, Feng JK, Si PC, Ci LJ (2018) Nanostructured $LiMn_2O_4$ composite as high-rate cathode for high performance aqueous Li-ion hybrid supercapacitors. J Power Sources 392:116–122
31. Qin QQ, Ou DW, Ye CJ, Chen LX, Lan BB, Yan J, Wu YC (2019) Systematic study on hybrid supercapacitor of Ni-Co layered double hydroxide//activated carbons. Electrochim Acta 305:403–415
32. Li JP, Xiao DS, Ren YQ, Liu HR, Chen ZX, Xiao JM (2019) Bridging of adjacent graphene/polyaniline layers with polyaniline nanofibers for supercapacitor electrode materials. Electrochim Acta 300:193–201
33. Meng G, Yang Q, Wu XC, Wan PB, Li YP, Lei XD, Sun XM, Liu JF (2016) Hierarchical mesoporous Nio nanoarrays with ultrahigh capacitance for aqueous hybrid supercapacitor. Nano Energy 30: 831–839
34. Wei MR, Che W, Li HZ, Wang ZH, Yan FW, Liu YH, Liu JP (2019) Ruddlesden-Popper type $La_2NiO_{4+\delta}$ oxide coated by Ag nanoparticles as an outstanding anion intercalation cathode for hybrid supercapacitors. Appl Surf Sci 484:551–559
35. Yu WD, Lin WR, Shao XF, Hu ZX, Li RC, Yuan DS (2014) High performance supercapacitor based on Ni_3S_2/carbon nanofibers and carbon nanofibers electrodes derived from bacterial cellulose. J Power Sources 272:137–143
36. Li LL, Peng SJ, Lee JKY, Jing DX, Srinivasan M, Ramakrishna S (2017) Electrospun hollow nanofibers for advanced secondary batteries. Nano Energy 39:111–139
37. Alali KT, Liu T, Liu JY, Liu Q, Fertassi MA, Li ZS, Wang J (2017) Preparation and characterization of ZnO/$CoNiO_2$ hollow nanofibers by electrospinning method with enhanced gas sensing properties. J Alloys Compd 702:20–30
38. Zhang YX, Ma D, Wu J, Zhang QZ, Xin YJ, Bao N (2015) One–step preparation of CNTs/$InVO_4$ hollow nanofibers by electrospinning and its photocatalytic performance under visible light. Appl Surf Sci 353:1260–1268
39. Santos-Gómez LD, Sanna S, Norby P, Pryds N, Losilla ER, Marrero-López D, Esposito V (2019) Electrochemical stability of (La,Sr)$CoO_{3-\delta}$ in (La,Sr)$CoO_{3-\delta}$/(Ce,Gd)$O_{2-\delta}$ heterostructures. Nanoscale 11:6
40. Singh RN, Tiwari SK, Singh SP, Singh NK, Poillerat G, Chartier P (1996) Synthesis of (La, Sr)CoO_3 perovskite films via a sol-gel route and their physicochemical and electrochemical surface characterization for anode application in alkaline water electrolysis. J Chem Soc Faraday Trans 92:2593–2598
41. Ahvenniemi E, Matvejeff M, Karppinen M (2015) Atomic layer deposition of quaternary oxide (La,Sr)$CoO_{3-\delta}$ thin films. R Soc Chem: Dalton Trans 44:8001–8006
42. Niu WJ, He JZ, Wang YP, Sun QQ, Liu WW, Zhang LY, Liu MC, Liu MJ, Chueh YL (2020) A hybrid transition metal nanocrystal-embedded graphitic carbon nitride nanosheet system as a superior oxygen electrocatalyst for rechargeable Zn-Air batteries. Nanoscale 12:19644–19654
43. He JZ, Niu WJ, Wang YP, Sun QQ, Liu MJ, Wang KY, Liu WW, Liu MC, Yu FC, Chueh YL (2020) In-situ synthesis of hybrid nickel cobalt sulfide/carbon nitrogen nanosheet composites as highly efficient bifunctional oxygen electrocatalyst for rechargeable Zn-air batteries. Electrochim Acta 362:136968
44. Wang YY, Lei Y, Li J, Gu L, Yuan H, Xiao D (2014) Synthesis of 3D-nanonet hollow structured Co_3O_4 for high capacity supercapacitor. ACS Appl Mater Interfaces 6:6739–6747
45. Cao Y, Lin BP, Sun Y, Yang H, Zhang XQ (2015) Symmetric/asymmetric supercapacitor based on the perovskite-type lanthanum cobaltate nanofibers with Sr-substitution. Electrochim Acta 178: 398–406
46. Xing L, Dong YD, Hu F, Wu X (2018) Co_3O_4 nanowire@NiO nanosheet arrays for high performance asymmetric supercapacitors. Dalton Trans 47:5687–5694
47. Yang PH, Mai WJ (2014) Flexible solid-state electrochemical supercapacitors. Nano Energy 8:274–290
48. Brousse T, Bélanger D, Long JW (2014) To be or not to be pseudocapacitive. Electrochem Soc 162:5185–5189
49. Kumar M, Subramania A, Balakrishnan K (2014) Preparation of electrospun Co_3O_4 nanofibers as electrode material for high performance asymmetric supercapacitors. Electrochim Acta 149:152–158

50. Xu XW, Yang Y, Wang M, Dong P, Baines R, Shen JF, Ye MX (2016) Straightforward synthesis of hierarchical Co_3O_4@$CoWO_4$/rGO core–shell arrays on Ni as hybrid electrodes for asymmetric supercapacitors. Ceram Int 42:10719–10725
51. Babu IM, William JJ, Muralidharan G (2019) Ordered mesoporous Co_3O_4/CMC nanoflakes for superior cyclic life and ultra high energy density supercapacitor. Appl Surf Sci 480:371–383
52. Khalaj M, Sedghi A, Miankushki HN, Golkhatmi SZ (2019) Synthesis of novel graphene/Co_3O_4/polypyrrole ternary nanocomposites as electrochemically enhanced supercapacitor electrodes. Energy 188:116088

Publisher's note Springer Nature remains neutral with regard to jurisdictional claims in published maps and institutional affiliations.